Supplemental material for "Volume changes during active shape fluctuations in cells"

Alessandro Taloni,[1,2] Elena Kardash,[3] Oguz Umut Salman,[1,4] Lev Truskinovsky,[5] Stefano Zapperi,[2,1,6,7,*] and Caterina A. M. La Porta[8,†]

[1]*CNR - Consiglio Nazionale delle Ricerche, Istituto per l'Energetica e le Interfasi, Via R. Cozzi 53, 20125 Milano, Italy*
[2]*Center for Complexity & Biosystems and Department of Physics, University of Milano, via Celoria 16, 20133 Milano, Italy*
[3]*Departments of Biochemistry and Molecular Biology, Sciences II, 30 Quai Ernest-Ansermet, CH-1211 Geneva 4, Switzerland*
[4]*CNRS, LSPM UPR3407, Université Paris 13, Sorbonne Paris Cité, 93430 Villetaneuse, France*
[5]*LMS, CNRS-UMR 7649, Ecole Polytechnique, Route de Saclay, 91128 Palaiseau, France*
[6]*Institute for Scientific Interchange Foundation, Via Alassio 11/C, 10126 Torino*
[7]*Department of Applied Physics, Aalto University, P.O. Box 14100, FIN-00076, Aalto, Finland*
[8]*Center for Complexity & Biosystems and Department of Bioscience, University of Milano, via Celoria 26, 20133 Milano, Italy*

METHODS

Zebrafish maintenance

Zebrafish (Danio Rerio) of the AB and AB/TL genetic background were maintained, raised and staged as previously described [1, 2].

Constructs and mRNA synthesis

For protein over-expression in germ cells, the mRNA was injected into the yolk at one-cell stage. Capped sense RNA was synthesized with the mMessage mMachine kit (Ambion, http://www.ambion.com/index.html). To direct protein expression to PGCs, the corresponding open reading frames (ORFs) were fused upstream to the 3UTR of the nanos1 (nos1-3UTR) gene, facilitating translation and stabilization of the RNA in these cells [3]. For global protein expression, the respective ORFs were cloned into the pSP64TS ector that contains the 5 and 3 UTRs of the Xenopus Globin gene. The injected RNA amounts are as provided below. The following constructs were used:

- YPet-YPet-RasCAAX-nos-1 (240 pg.) was used to label membrane in germ cells.
- Lifeact-pRuby-nos-1 (240 pg.) was used to label actin in germ cells.
- DN-ROK-nos-1 (300 pg.) was used to interfere with ROK function in PGCs
- Aqp1a-nos-1 (300 pg.) was used to over-express aquaporin-1a in PGCs
- Aqp3a-nos-1 (300 pg.) was used to over-express aquaporin-3a in PGCs
- Aqp1aEGFP-nos-1 (360 pg.) was used to visualize the subcellular localization of aquaporin1a in PGCs
- Aqp3aEGFP-nos-1 (300pg.) was used to visualize the subcellular localization of aquaporin3a in PGCs

Morpholino knockdown

The morpholinos for knocking down protein translation were obtained from GeneTools, LLC http://www.gene-tools.com/. The following sequences were used: Aquapoin1a: 5 AAGCCTTGCTCTTCAGCTCGTTCAT3 (injected at 400μM); Aquaporin 3a: 5 ACGCTTTTCTGCCAACCCATCTTTC 3 (injected at 400μM);. For the control, standard morpholino 5CCTCTTAC-CTCAGTTACAATTTATA 3 was used.

Live Imaging of germ cells in zebrafish embryos

Time-lapse movies of blebbing cells in live zebrafish embryos were acquired with the Zeiss LSM710 bi-photon microscope using one-photon mode. The 20x water-dipping objective with the numerical aperture 1.0 was used. The bit depth used was 16 and the scanning speed ranged between 150 to 250 ms/frame for fast imaging of bleb formation.

Image processing

Images were preprocessed with Fiji software to eliminate the background. The Bleach Correction tool (EMBL) was used to correct for the reduction in fluorescence intensity during prolonged time-lapse movies. Sequences of of image stacks were then processed using the 3D Active Meshes algorithm [4] implemented in the Icy software http://icy.bioimageanalysis.org/. The algorithm performs three-dimensional segmentation and tracking using a triangular mesh that is optimized using the original signal as a target. From the resulting three dimensional mesh one can then measure the cell volume its surface area. Three dimensional rendering of the meshes was done using Paraview (http://www.paraview.org/).

Statistical analysis

Statistical significance was evaluated using Kolmogorov-Smirnov tests implemented in custom made python codes.

Test of the accuracy of cell volume evaluations

To confirm that the volume fluctuations observed in the zebrafish cells in vivo are real, we have to exclude possible systematic errors induced by the three dimensional mesh reconstruction algorithm [4]. Our experimental analysis shows smaller volume fluctuations for cells where the bleb formation has been suppressed (DN-ROK and AQP- mutants), with respect to wild type cells (WT) or those for which blebbing has been enhanced (AQP+). In particular, as shown in Fig. 1(a), WT and AQP+ cells display a more complex morphology when compared to DN-ROK or AQP-, which appear instead to have a rounded shape. Hence, the first question to be answered is whether in presence of complex morphological shapes, the algorithm introduces a systematic bias in the measured cell volume. In other words the question is: does the algorithm produce a larger error while calculating the volume of blebbing cells, with respect to those where blebs are absent?

To answer to this question we generate a set of synthetic ellipsoidal cells whose volume is in the range of the zebrafish cells analyzed in our experiments ($\sim 2000-3000\mu m^3$), as shown in Fig.S3. Synthetic cells are generated through the ImageJ software (http://imagej.nih.gov/ij/) by creating 3D stacks having the shape of ellipsoids with semi-axes a_x, a_y and a_z. Initially, we set the voxel size to $0.13\mu m$ along the three directions (see Fig.S3(a)). The volume is then calculated both according to the formula $V_{ell} = 4\pi/3 a_x a_y a_z$ and by counting the number of voxels belonging to the synthetic cell, V_{wp}. The relative error between the two estimates is $\langle \frac{V_{wp}-V_{ell}}{V_{ell}} \rangle \simeq -0.05\%$, so that we can safely consider the estimate V_{wp} as the real volume of the synthetic stacks generated. The main sources of error in analyzing confocal image stacks stems from the anisotropic voxel. In our experiments the resolution along the z direction is $0.78\mu m$, while it is $0.13\mu m$ in the xy plane. To reproduce the voxel anisotropy in the synthetic stacks, we select just one single xy plane every 6 composing the original z-stack. A resulting typical cell is shown in Fig.S3(b). We then extract the mesh of this newly obtained stack (see Fig.S3(c)) and calculate the ensuing volume $V_{no-bleb}$. Our set of synthetic cells consists of 35 ellipsoids of different semi-axes, for which we calculate the true volume V_{wp} reported in Fig.S4. Then, each ellipsoid is first processed by the anysotropic voxelization in the z direction, and subsequently analyzed by the 3D Active Mesh algorithm. The volumes of the extracted meshes are reported in Fig.S4 ($V_{no-bleb}$). It is apparent that the algorithm systematically underestimates the volume by roughly $\delta = \langle \frac{V_{no-bleb}-V_{wp}}{V_{wp}} \rangle \simeq -14\%$. We checked that is error is greatly reduced for isotropic voxels.

A constant systematic error is not worrying, since we are only interested in changes in volume and all the images have the same voxel anisotropy and therefore the same error. Before addressing the fluctuations of this error, we focus on possible spurious changes in the measured volume induced by a change in shape. For each of the synthetic ellipsoidal cells, we create a synthetic cell with the same volume but presenting 1, 2, or 3 blebs on the surface. Blebs are generated as spherical caps of different radii with centers placed randomly on the ellipsoid surface (see Fig.S3(d)). We then perform the same anysotropic voxelization of the original z-stack done for the plane ellipsoids (see Fig.S3(e)). From this image we extract the active mesh (Fig.S3(f)) and calculate its volume. The volumes of the meshes of synthetic cells with blebs, V_{bleb}, are displayed in Fig.S4. One can only see a very small difference between the values of V_{bleb} and $V_{no-bleb}$, but they both appear underestimate the true value V_{wp} by

about $\delta \simeq -14\%$. What is surprising, however, is that cells with blebs appear to approximate the real volume slightly better than cells without blebs. To confirm this, we report in Fig.S5 the relative volume fluctuations $\frac{V_{bleb}-V_{no-bleb}}{V_{no-bleb}}$ as a function of the measured mesh surface fluctuations $\frac{\Sigma_{bleb}-\Sigma_{no-bleb}}{\Sigma_{no-bleb}}$. If no errors were made by the algorithm in estimating the synthetic volumes one would expect $\frac{V_{bleb}-V_{no-bleb}}{V_{no-bleb}} = 0$ since pair of cells were constructed with the same volume but different shapes. If complex shape with blebs would lead to an overestimation of the volume with respect an ellipsoidal cell with no blebs, one would expect $\frac{V_{bleb}-V_{no-bleb}}{V_{no-bleb}}$ and $\frac{\Sigma_{bleb}-\Sigma_{no-bleb}}{\Sigma_{no-bleb}}$ to be positively correlated. To the contrary, the linear regression of the data in Fig.S5 shows a small but clear anti-correlation between volume and surface fluctuations. This is in contrast with experimental results showing that changes in shape are positively correlated with changes in volume (Fig. S7). Hence, this result can not be considered an artefact of the measurement but a real feature of the cells.

The previous analysis clearly demonstrates that the volume fluctuations observed in our experiments do not depend on the shape of the cells, but the algorithm systematically underestimates the volume of both of about $\delta \simeq -14\%$. The next question is whether these systematic fluctuations are of the same order of magnitude as the observed ones. Are the fluctuations reported in Fig. 1(b) real or just an artefact introduced by the mesh reconstruction algorithm? This question is particularly compelling in the case of WT and AQP+ cells, since for DN-ROK and AQP- cells we can accept that the volume might remain constant. To answer to this question generate a set of 120 synthetic cells, 60 with blebs randomly placed and of different sizes, and 60 without blebs, each cell having its own real volume V_{wp} calculated with ImageJ. We then process each synthetic cell according to the protocol previously outlined: anysotropic voxelization in the z direction and subsequent mesh analysis. Finally we calculate the fluctuations $\frac{\Delta V}{\overline{V}} = \frac{V_{(no-)bleb}-V_{wp}}{V_{wp}}$ and its cumulative distribution $P\left(\frac{\Delta V}{\overline{V}}\right)$. In Fig.S6 we compare $P\left(\frac{\Delta V}{\overline{V}}\right)$ with the corresponding cumulative distributions of WT, AQP+, DN-ROK and AQP- cells, once it has been shifted by the average systematic volume bias $\delta \simeq -14\%$. This figure shows that systematic errors made by Icy in the estimation of the cell volume, are compatible with the observed volume fluctuations of DN-ROK and AQP- cells, but not with those AQP+ and WT cells, which instead appear to be significantly larger. We thus conclude that the difference in volume fluctuation between AQP+/WT cells and DN-ROK/AQP- is not an artefact of the analysis.

Volume conservation in numerical simulation

By performing numerical simulations, we notice that a straightforward formulation of the method suffers from poor volume conservation. This general drawback of the immersed boundary method has been already pointed out by many other authors in different contexts [5, 6]. To overcome this problem we implement the method proposed in Ref. [6] and enforce the incompressibility constraint on the discrete Lagrangian grid in the weak sense:

$$\sum_{k=1}^{N} \mathbf{u}(\mathbf{r}_{\mathrm{m}_k}) \cdot \mathbf{n}(\mathbf{r}_{\mathrm{m}_k}) \Delta S(\mathbf{r}_{\mathrm{m}_k}) = 0, \tag{S1}$$

where $\mathbf{n}(\mathbf{r}_{\mathrm{m}_k})$ is the outward unit normal to the membrane at the position $\mathbf{r}_{\mathrm{m}_k}$ and $\Delta S(\mathbf{r}_{\mathrm{m}_k})$ is a discrete measure of the arclength in the actual configuration at the position $\mathbf{r}_{m_k}$. The above constraint is satisfied by adding a corrective term to the equation of motion $\dot{\mathbf{r}}_{\mathrm{m}_k} = u^{\mathrm{corr}}(\mathbf{r}_{\mathrm{m}_k})$, where $u^{\mathrm{corr}} \equiv u(\mathbf{r}_{\mathrm{m}_k}) - M\mathbf{n}(\mathbf{r}_{\mathrm{m}_k})$ satisfies the incompressibility constraint and M is given by

$$M = \frac{1}{\sum_{i=1}^{N} \Delta S(\mathbf{r}_{\mathrm{m}_i})} \sum_{k=1}^{N} \mathbf{u}(\mathbf{r}_{\mathrm{m}_k}) \cdot \mathbf{n}(\mathbf{r}_{\mathrm{m}_k}) \Delta S(\mathbf{r}_{\mathrm{m}_k}). \tag{S2}$$

With this correction, we observe that the incompressibility constraint is satisfied and the cell volume is perfectly conserved.

SUPPLEMENTAL FIGURES

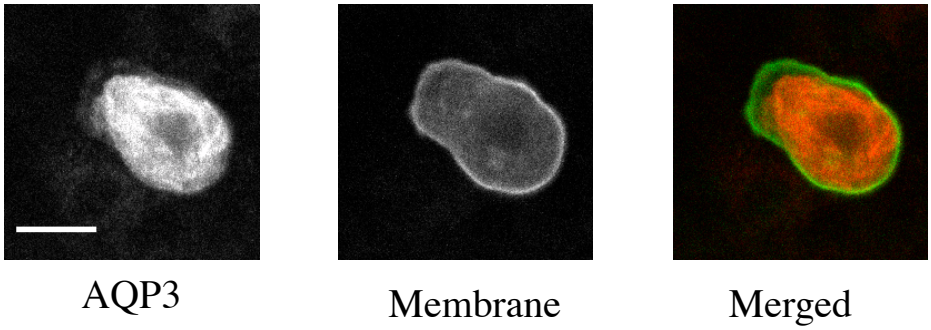

FIG. S1: AQP3 is expressed by PGCs. A PGC expressing EGFP fusion of Aquaporin-3a and an RFP-tagged membrane marker. Scale bar is 10μm.

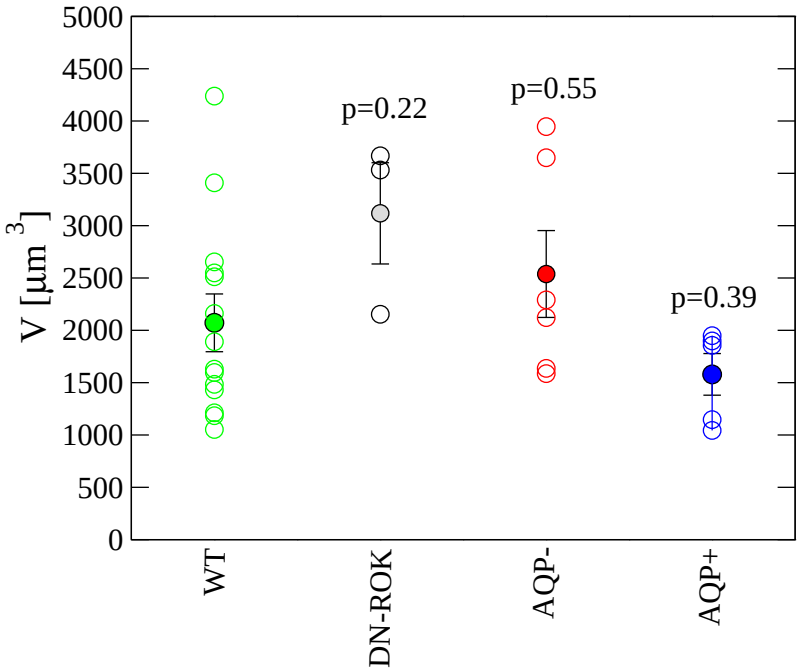

FIG. S2: Aquaporin knockdown and overexpression does not induce significant changes in the average cellular volume. A similar result holds for the DN-ROK mutant. The results show the dispersion of the data, the average and the standard error. Statistical significance (p values) is evaluated according to the Kolmogorov-Smirnov test.

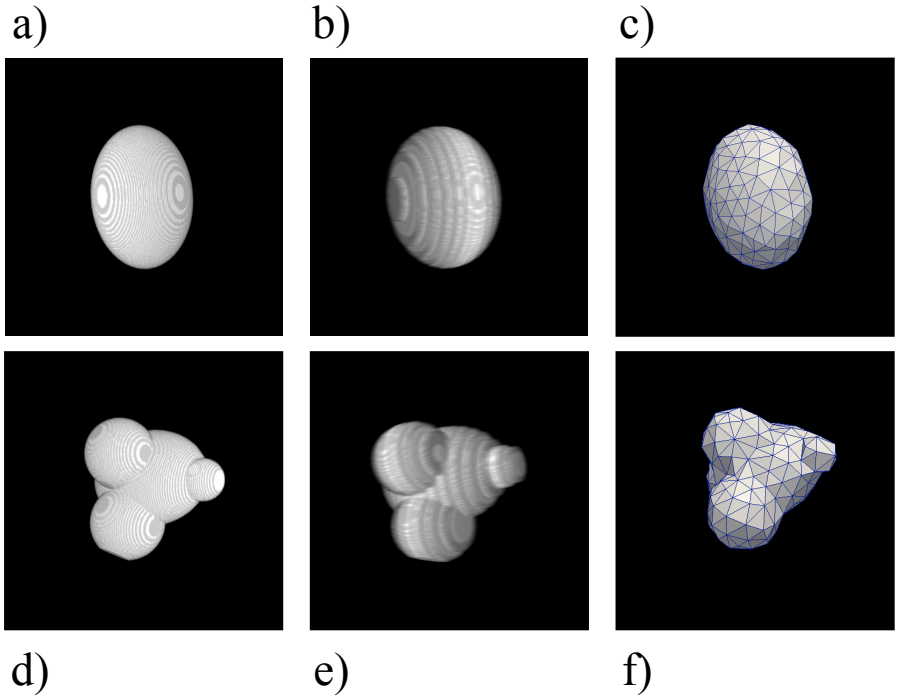

FIG. S3: Two example of synthetic image stacks representing cells without (a-c) and with (d-f) blebs. The original stacks of equal volume (a and d), are first transformed removing a set of planes (1 every 6) to obtain an anisotropic voxel corresponding to the experimental resolution (b and e), i.e. 0.13μm in the x,y directions and 0.78μm along z. The resulting stacks (b and e) are analyzed to obtain a three-dimensional mesh (shown in c and f)

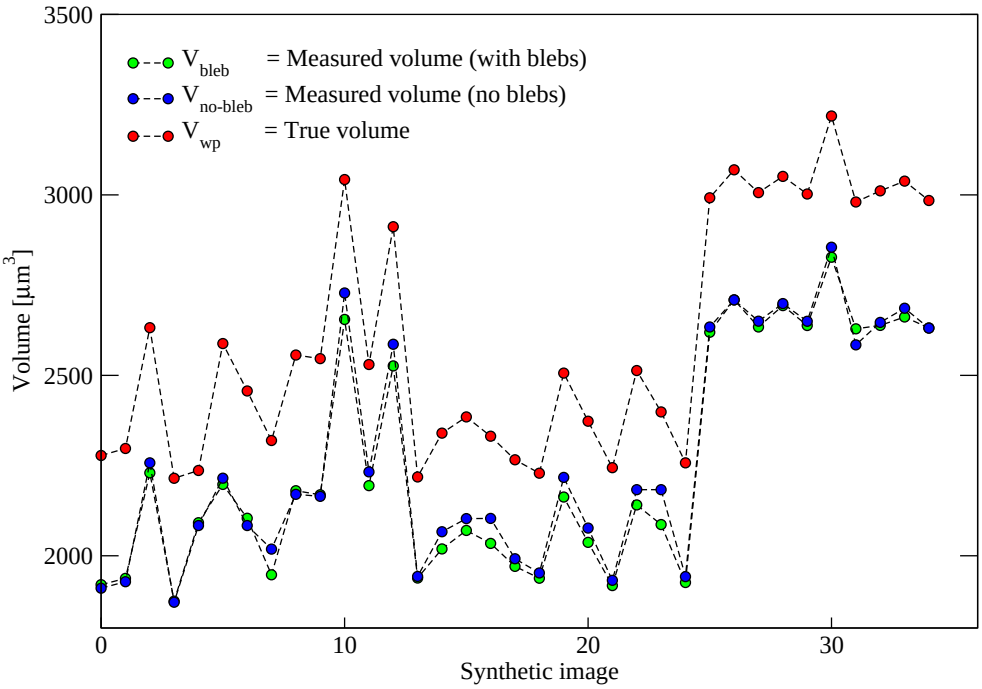

FIG. S4: Volume comparison of synthetic cells. We compare the measured volumes of cells without blebs ($V_{no-bleb}$) with those corresponding to cells with blebs (V_{bleb}) and with the true volumes (V_{wp}), which is the same for each pair of cells. The results show a large constant systematic error $\delta \simeq -14\%$, and small fluctuations for cells with and without blebs.

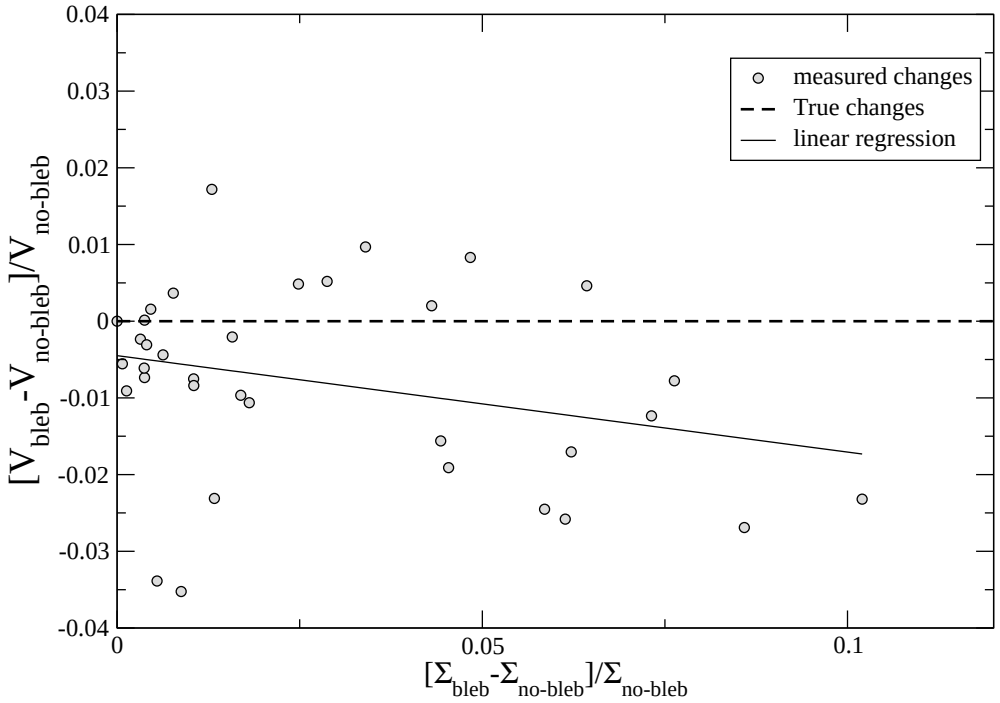

FIG. S5: The relative difference in the measured volume for pairs of cells of the same true volume but different surface due to the presence or absence of blebs. The data show fluctuations of 1% and a small negative correlation between volume and surface changes.

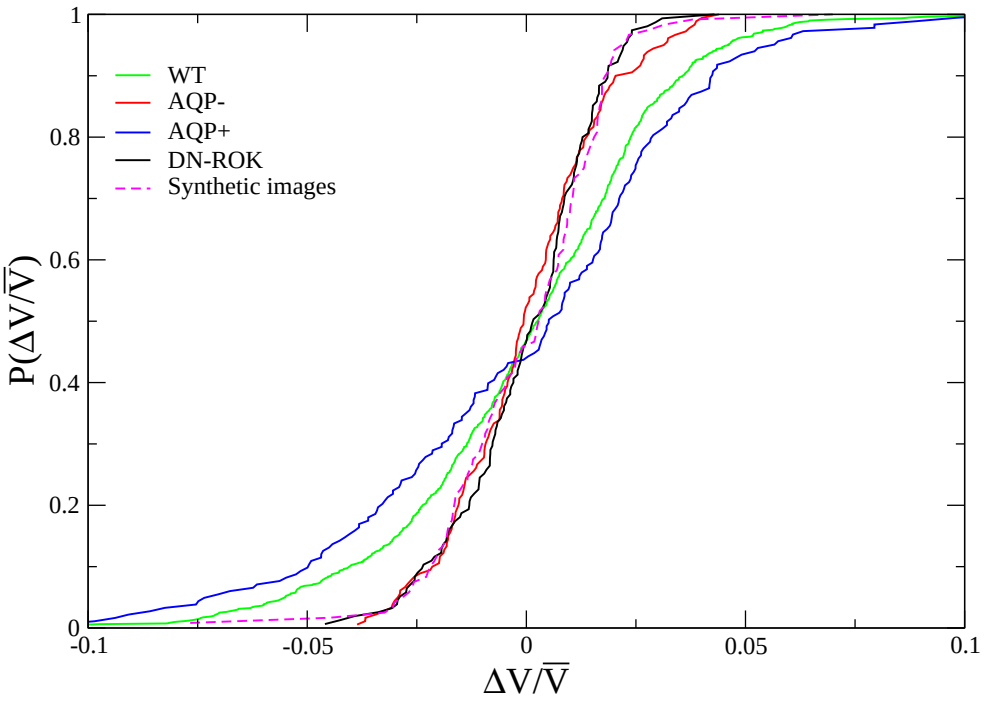

FIG. S6: The cumulative distribution of relative error fluctuations for the volume of a large number of synthetic cells with and without blebs compared with experimental measurements. The cumulative distribution of synthetic cells is shifted by $-\delta$ to allow a visual comparison with the experimental quantities. $\overline{V}$ corresponds the time averaged volume for AQP+, AQP-, DN-ROK and WT cells, whilst it is $\overline{V} = V_{wp}$ for synthetic cells. Volume fluctuations for WT and AQP+ cells are significantly larger than those observed in synthetic cells, whereas DN-ROK and AQP- mutant cells volume fluctuations seem to be compatible with the systematic errors induced by the mesh algorithm.

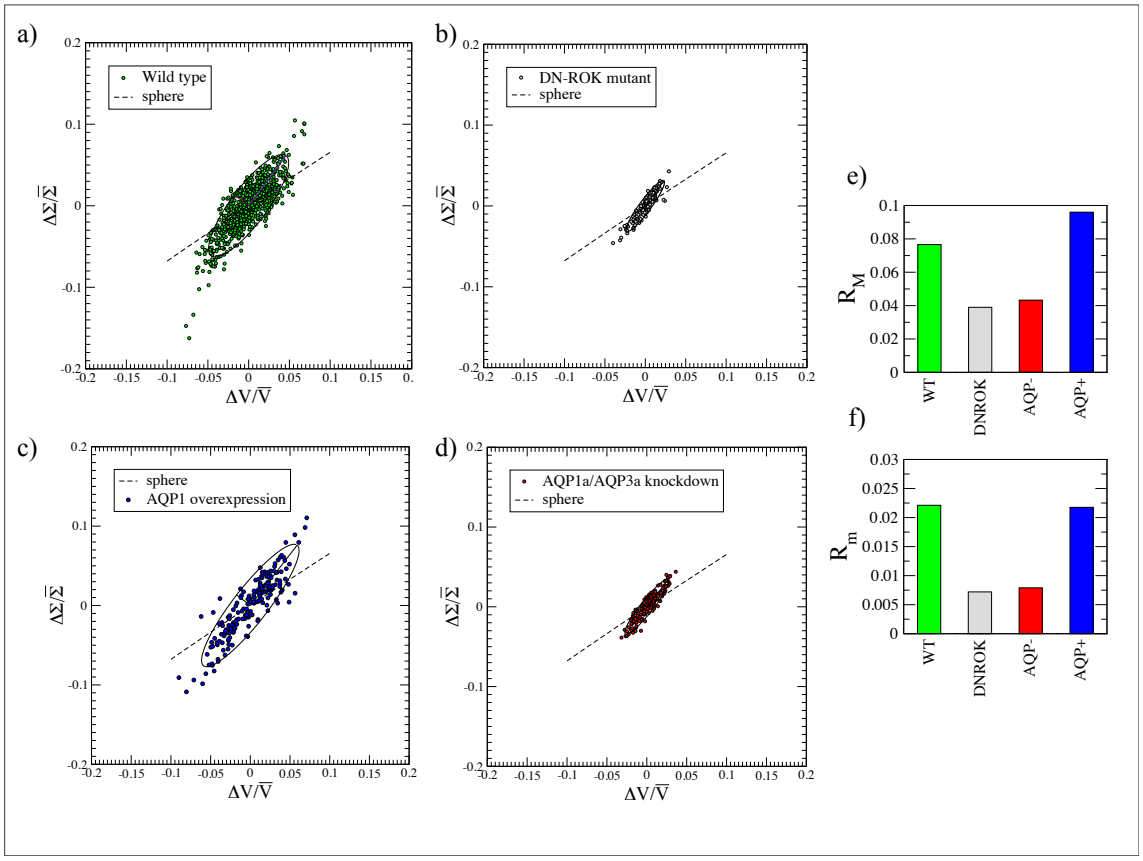

FIG. S7: Volume and surface fluctuations are correlated. Principal component analysis of volume and surface relative values. Scatter plots for a) WT, b) DN-ROK, c) AQP+ and d) AQP- are reported together with an ellipse with axis given by the two eigenvectors of the cross-correlation matrix, whose amplitude is reported in panel e) and f) for the largest and smaller axis. The dashed line represents the expected result for the ideal case of the isotropic deformation of a sphere.

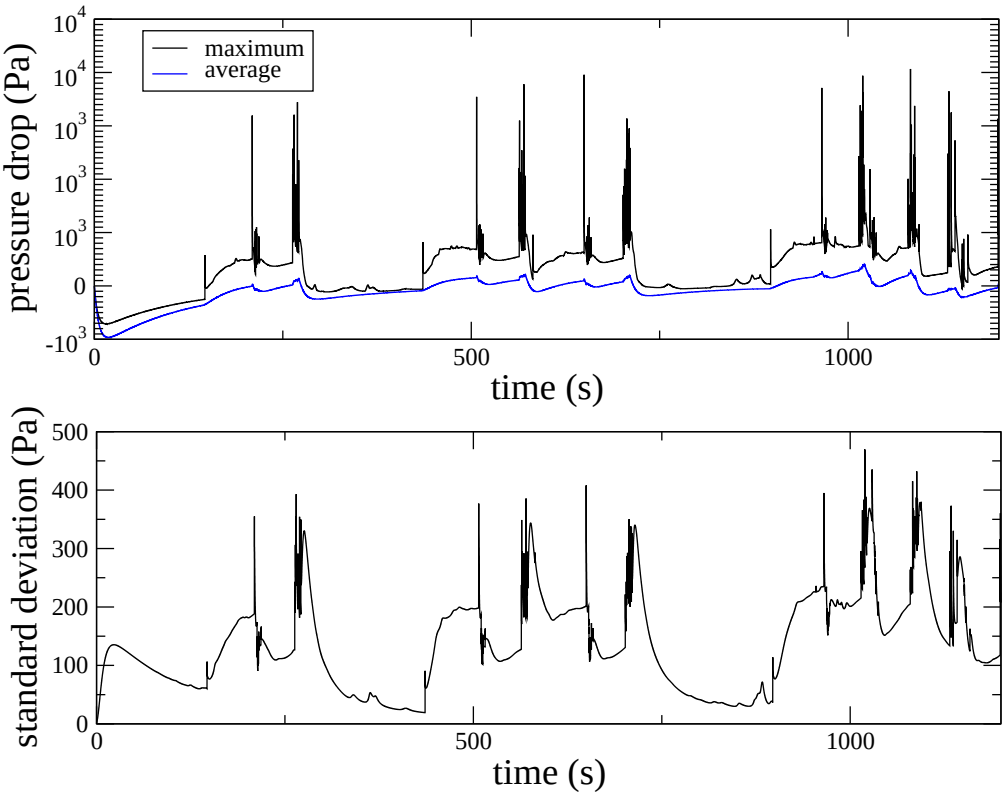

FIG. S8: Time evolution of the pressure drop across the membrane from numerical simulations.A representative example of the evolution of the pressure drop in numerical simulations shows that the average is very different from the maximum (top). Furthermore, the standard deviation of the distribution fluctuates intermittently in time in correspondence to the blebbing activity (bottom). Results are obtained for a permeability $\alpha = 2 \cdot 10^{-14} \mathrm{m}^2\mathrm{s}/\mathrm{kg}$.

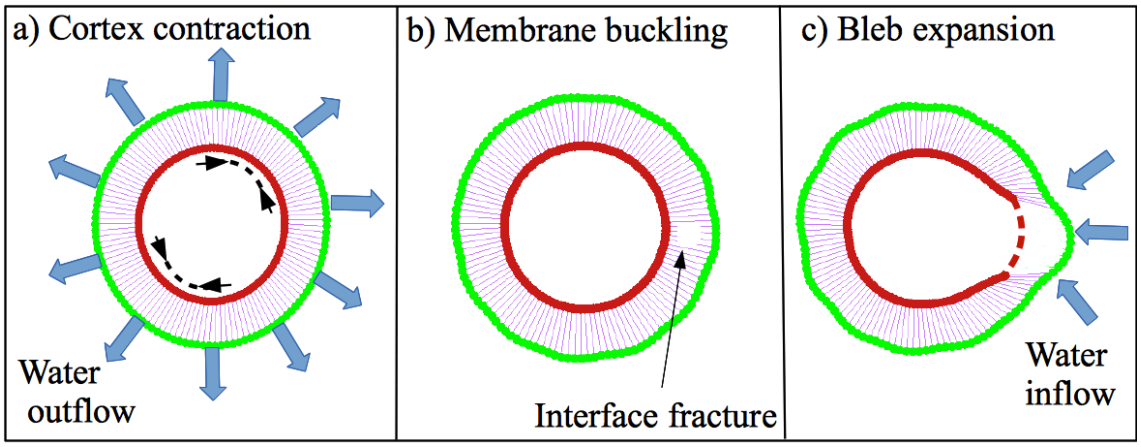

FIG. S9: A schematic representation of the bleb formation process. a) The cortex contracts squeezing water outside of the cell. b) The membrane buckles and the cortex-membrane interface fractures. c) The bleb expands as the interface fails and water flows inside the cell as the internal fluid pressure is relieved.

SUPPLEMENTAL TABLES

	WT	DNROK	AQP-	AQP+
p-value ($\Delta V/\bar{V}$)	0.11	0.21	0.17	0.99
p-value ($\Delta\Sigma/\bar{\Sigma}$)	0.68	0.75	0.7	0.13

TABLE I: Results of statistical significance tests for validity of Gaussian statistics for volume and surface fluctuations. We report the p-values obtained from the Kolmogorov-Smirnov test. A small p-value (e.g. $p < 0.01$) would imply that we can reject the hypothesis that the distribution is described by Gaussian statistics. In the present case, the p-value is large indicating that a Guassian distribution provides a good fit to the data.

	WT / DNROK	WT/ AQP-	WT/ AQP+	AQP-/ DNROK	AQP+/ AQP-	AQP+/ DNROK
p-value ($\Delta V/\bar{V}$)	$5 \cdot 10^{-5}$	$4 \cdot 10^{-4}$	0.25	0.62	$8 \cdot 10^{-5}$	$8 \cdot 10^{-5}$
p-value ($\Delta\Sigma/\bar{\Sigma}$)	0.001	0.008	0.09	0.98	$6 \cdot 10^{-6}$	$6 \cdot 10^{-6}$

TABLE II: Results of statistical significance tests for the comparison between WT, DNROK,AQP+,AQP- cells in the case of volume and surface distributions. We report the p-values obtained from the Kolmogorov-Smirnov test. A low p-value (e.g. $p < 0.01$) indicates that we can reject the hypothesis that the two data sets are described by the same distribution.

Symbol	Quantity	Value	Reference
r_{m}	membrane radius	$25\ \mu\mathrm{m}$	[7]
r_{c}	cortex radius	$24\ \mu\mathrm{m}$	[7]
$\epsilon_{\mathrm{c}} = \epsilon_{\mathrm{m}}$	rest length of cortex/membrane elements	$1.3\ \mu\mathrm{m}$	—
Δ	regularization parameter	$0.5 \times \epsilon$	[8]
k_{m}	membrane stiffness coefficient	$6 \times 10^{-6}\ \mathrm{Nm}^{-1}$	[9]
k_{c}	cortex stiffness coefficient	9×10^{-5}	[9]
B_{m}	membrane flexural rigidity	$4 \times 10^{-20}\ \mathrm{J}$	[9]
B_{c}	cortex flexural rigidity	$2.8 \times 10^{-19}\ \mathrm{J}$	[9]
k_{mc}	cortex-membrane interface stiffness	$25 \times 10^{-6}\ \mathrm{Nm}^{-3}$	[9]
μ_{c}	cortex drag coefficient	$10^{-7}\ \mathrm{kgm}^{-2}\mathrm{s}^{-1}$	[10]
ν_{c}	cortex healing speed	$6 \times 10^{-4}\ \mathrm{ms}^{-1}$	[11]
μ	Cytosolic viscosity	$10^{-1}\ \mathrm{kgm}^{-1}\mathrm{s}^{-1}$	[11]
α	membrane permeability	$10^{-4} - 10^{-1} \times 10^{-12}\ \mathrm{m}^2\mathrm{skg}^{-1}$	[12]

TABLE III: Parameters employed in numerical simulations

SUPPLEMENTAL MOVIE CAPTIONS

Movie S1 A representative example of the time evolution of a PGC in WT conditions. The movie is obtained using an average intensity 3D projection in imageJ.

Movie S2 A representative example of the time evolution of a PGC in DNROK conditions. The movie is obtained using an average intensity 3D projection in imageJ.

Movie S3 A representative example of the time evolution of a PGC in AQP- conditions. The movie is obtained using an average intensity 3D projection in imageJ.

Movie S4 A representative example of the time evolution of a PGC in AQP+ conditions. The movie is obtained using an average intensity 3D projection in imageJ.

Movie S5 A simulation of the computational model using a porous membrane. The color represents fluid pressure (see Fig. 3a).

Movie S6 A simulation of the computational model using an impermeable membrane. The color represents fluid pressure (see Fig. 3b).

* Electronic address: stefano.zapperi@unimi.it
† Electronic address: caterina.laporta@unimi.it

[1] M. Westerfield, *The zebrafish book: A guide for the laboratory use of zebrafish (Danio rerio)* (Univ. of Oregon Press, Eugene, 1993).
[2] C. B. Kimmel, W. W. Ballard, S. R. Kimmel, B. Ullmann, and T. F. Schilling, Dev Dyn **203**, 253 (1995).
[3] M. Köprunner, C. Thisse, B. Thisse, and E. Raz, Genes Dev **15**, 2877 (2001).
[4] A. Dufour, R. Thibeaux, E. Labruyère, N. Guillén, and J.-C. Olivo-Marin, IEEE Trans Image Process **20**, 1925 (2011).
[5] J. M. Stockie, Computers & Structures **87**, 701 (2009).
[6] E. P. Newren, Ph.D. thesis, Dept. of Mathematics, University of Utah (2007).
[7] J.-Y. Tinevez, U. Schulze, G. Salbreux, J. Roensch, J.-F. Joanny, and E. Paluch, Proc Natl Acad Sci U S A **106**, 18581 (2009).
[8] R. Cortez, SIAM Journal on Scientific Computing **23**, 1204 (2001).
[9] G. T. Charras, M. Coughlin, T. J. Mitchison, and L. Mahadevan, Biophys J **94**, 1836 (2008).
[10] W. Strychalski and R. D. Guy, Math Med Biol **30**, 115 (2013).
[11] F. Y. Lim, Y. L. Koon, and K.-H. Chiam, Comput Methods Biomech Biomed Engin **16**, 1085 (2013).
[12] M. Hagedorn, F. W. Kleinhans, R. Freitas, J. Liu, E. W. Hsu, D. E. Wildt, and W. F. Rall, J Exp Zool **278**, 356 (1997).